Pot-ability Assessment of Litz Wires for High Power Density Electric Motor

Euy-Sik Eugene Shin[1]
Ohio Aerospace Institute, NASA Glenn Research Center, 21000 Brookpark Rd., MS 49-1, Cleveland, OH 44135, USA

An alternative process technique, namely vacuum-assisted axial injection potting (VaAIP), has been developed to pot the Litz wires in the stator winding of high power density electric motors for the future electrified aircrafts. Initial trials of the process showed significant improvement in potting quality with less voids, thus potential improvement in thermal management of the motors. As an initial effort of pot-ability assessment, microstructures, 2-D and 3-D, of the Litz wires including dimensions and distribution of conductor filament, coating, and open spaces; packing patterns; shape/configuration changes of each bundles or the overall cross-sections per degree of twist were determined and quantified successfully. The microstructure analyses were performed not only for effective potting process development but also for more realistic electro-thermal modeling solutions. This paper will present results of the microstructure analyses, potentials of the VaAIP process from the trials, and future plans for scale-up and implementation of the process into a full-scale prototype stator winding.

Nomenclature

2-D = *2*-Dimensional
3-D = 3-Dimensional
AWG = American Wire Gage
BF = Bright Field
BNNS = Boron Nitride Nano-Sheet
CF = Conductor Filament
DF = Dark Field
FT-IR = Fourier Transform-Infrared Spectroscopy
HEMM = High Efficiency Megawatt Motor
PI = Polyimide
VaAIP = Vacuum-assisted Axial Injection Potting
VPI = Vacuum Pressure Impregnation

I. Introduction

ONE of the challenging tasks in developing high efficiency and high power density electric motors for the future electrified aircraft application as summarized in Ref. [1] is the improved thermal management of the motor building blocks such as stator winding. Typical Litz wires consisting of thousands of fine conductor filaments regularly twisted in several bundles have been considered for the stator winding with benefit of reducing AC losses and the skin effect in high frequency windings, Ref. [2]. To increase the rate of heat dissipation from the core of conductor windings to motor casing, the Litz wire has to be fully filled with dielectric potting compound with relatively high thermal conductivity. The potting also provides mechanical stability of the stator windings and eliminates potential internal partial discharge by removing free space between wires which possibly cause micro plasmas formation between the wires, thus successful potting is an essential part of the future electric motor development (Ref. [1]). The work presented in this paper focused on assessing pot-ability of the Litz wires with commercial potting compounds, developing more practical and effective potting processes, and also improving thermal conductivity of the potting compound.

[1] Principal Scientist, Research Team Manager-Materials, Ohio Aerospace Institute (OAI). On-site contract researcher at NASA GRC. Non-AIAA member.

II. Experimental

A. Materials

Two types of Litz wires investigated in this work were designed and manufactured by the New England Wire technologies (NEWT, Lisbon, NH) and designated as Litz1 and Litz2 as shown in Figure 1. Both were rectangular type 8 Litz wire and 3 AWG equivalent. The former was built by 5(5/6/108/44 Bare Copper), single Nylon for bundle insulation, and single Nomex for external wire insulation while the latter was by 4(5/5/60/40 Natural Single Polyimide (MW16-C), single Nylon for bundle insulation, and double Nomex for external wire insulation. Thus, the main differences between the two Litz wires were CF gage (44 AWG/50 µm Ø vs. 40 AWG/80 µm Ø), number of bundles (5 vs. 4), number of filaments per bundle (3,240 vs. 1,500), and wire insulation coating (no coating vs. PI coating).

The potting resin selected for this experiment and for the project was Durapot™ 863 from Cotronics Corp, Brooklyn, NY. The Durapot™ 863 is unfilled two part potting epoxy and has unique properties stemming from their proprietary crosslinked, inorganic-organic polymer system, such as low viscosity and exceptionally high thermal conductivity of 1.3 W/mK. It can be cured by the standard cure cycle, 4 hours at 121 °C/250 °F or by an accelerated cure cycle, 1 – 2 hours at 177 °C/350 °F. It is a 100 % reactive and can be used to 343 °C/650°F if cured by the latter. Based on its temperature-time-viscosity relation determined by systematic rheological analysis, the mixed epoxy has a viscosity of ~2000 cps at room temperature, but it drops to ~600 cps at 50 °C and further to 200-300 cps at 70 °C.

B. Image Analysis

Samples for high magnification/resolution image analysis were prepared by the typical metallurgical polishing after encapsulating with a mounting resin, usually a fluorescent epoxy in order to distinguish from the wire potting epoxy. A high power inverted optical microscope (Eclipse MA200, Nikon Metrology NV) was used to conduct in-situ image analyses on the polished surfaces or to acquire high magnification high resolution images of specific areas or the entire cross-section using the scan large image function, which is an automatic stitching process, for other post analyses. The resolution of the stitched images was determined by the magnification of the objective lense, but typically 10x lens was used for optimum quality and manageable file size per image, ~ 1 gigabyte, which allowed up to 100x zoomed-in view with good resolution in a computer monitor, as shown in Figure 1(c). The images were viewed or taken under either bright field or dark filed or both with altering exposure time depending on type of structural features. As a post analysis, the high resolution images were then imported into an ImageJ software (Fiji, an open source image processing package, https://imagej.net/Fiji) for more sophisticated structural analyses.

3-dimensional microstructure analyses of the wires were carried out by a serial polishing, either manually or with a fully-automated serial sectioning system (ROBO-MET.3D, UES Inc., Dayton, OH) as well as by an optical sectioning technique using an X-ray microfocus-Computed Tomography (µCT). An XRay WorX SE-225 (160 kV, 100 µA) microfocus x-ray source with Dexela 2923 detector, Ref. [3], was used to acquire multiple x-ray projection images. Then, the crosssectional slices of the part were obtained from the projection images by software reconstruction techniques. The cross-sectional images could be viewed individually or used to render a volume. The µCT scan did not require any sample preparation unlike the serial polishing. The ImageJ software was also used to render a volume or 3-dimensional views.

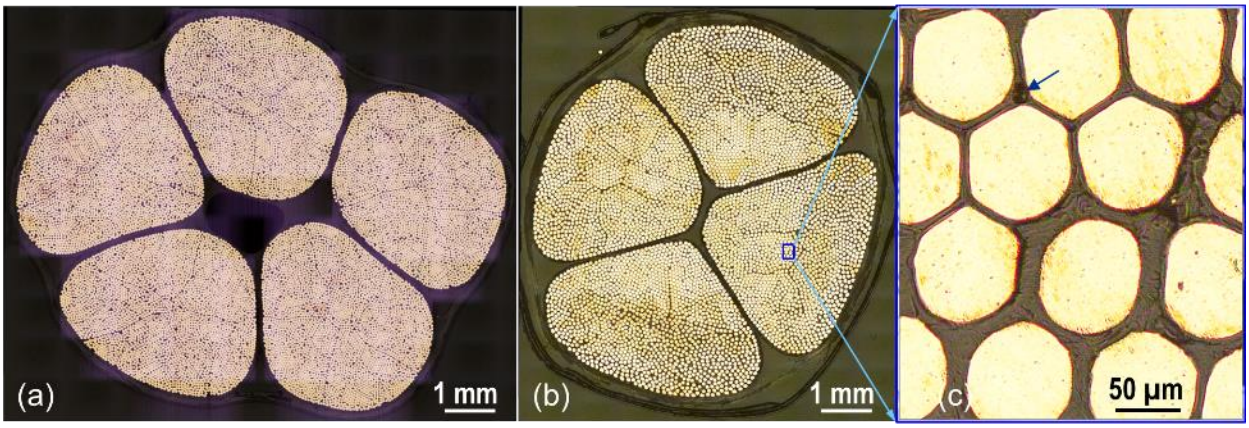

Figure 1. Cross-sectional micrographs of two candidate Litz wires, (a) Litz1, (b) Litz2, and (c) 30x Zoomed-in image with good resolution in computer monitor, showing a small void at the arrow mark.

C. Molecular Structure Analysis

FT-IR in Both ATR mode (380/Nicolet) and a noncontact scanning method via reflection mode (Nicolet NEXUS 670 with Thermo Nicolet Continuum microscope) was employed to assess the changes in molecular structure of the potting epoxy in terms of the degree of cure. The former was used for flat samples of the potting epoxy alone undergone various degrees of cure by controlling cure time while the latter was used to focus the small center area of the epoxy in the cross-sections of the potted Litz2 wire. The IR microscope had a zooming capacity up to ~200X.

III. Results and Discussions

A. Characterization of Microstructure

As the initial effort of pot-ability assessment, configuration and microstructure of the wires, particularly packing patterns and distribution characteristics of CFs and inter-filament open spaces, such as dimensions and overall areal or volume fraction, were determined from numerous cross-sections. Since shape/configuration of each bundles or the overall cross-sections changed considerably with degree of twist or mounting conditions, great care was taken to keep the maximum twisting of wire sections during sample preparations. From the overall cross-sectional analysis, it was observed that distribution of CFs in Litz1 was generally homogenous but Litz2 wire formed two distinctive patterns, i.e., denser packing in inner area of bundles toward the wire center vs. more loosely packed outside area in all four bundles as shown in Figure 1. While it was not clear whether the non-uniformity was caused by wire manufacturing conditions/procedures or simply due to bundle geometry, the patterns in Litz2 wire were consistent regardless of sample preparation or mounting conditions. Since the Litz2 wire was selected as the final candidate for a GRC demonstrator motor, High Efficiency Megawatt Motor (HEMM), Ref [4], the effects of the non-uniformity on overall power density of conductor windings or more importantly heat dissipation optimization will be systematically examined. Figure 2 shows typical CF arrangement patterns of the Litz wires in higher magnification. The patterns in Litz1 wire, either regularly ordered structure, top picture in Figure 2(a), or random, bottom picture in Figure 2(a), were fairly uniform throughout the entire bundles as expected from the overall cross-sectional views. Size of open spaces ranged from hundreds of micron to only a couple of microns in various shapes. In the case of Litz2 wire, the three phases, CF, coating, and open space, were clearly visible in the loosely packed area, left pictures in Figure 2(b), but in the more densely packed areas, sometimes there were no visible open spaces between CFs and furthermore, some filaments were deformed into hexagonal shape only separated by the coating layers, right pictures in Figure 2(b). This suggested that CFs in the inner area were subjected to substantially high packing forces. In general, however, the open spaces in Litz2 wire were slightly larger due to larger filaments compated to those in Litz1 wire.

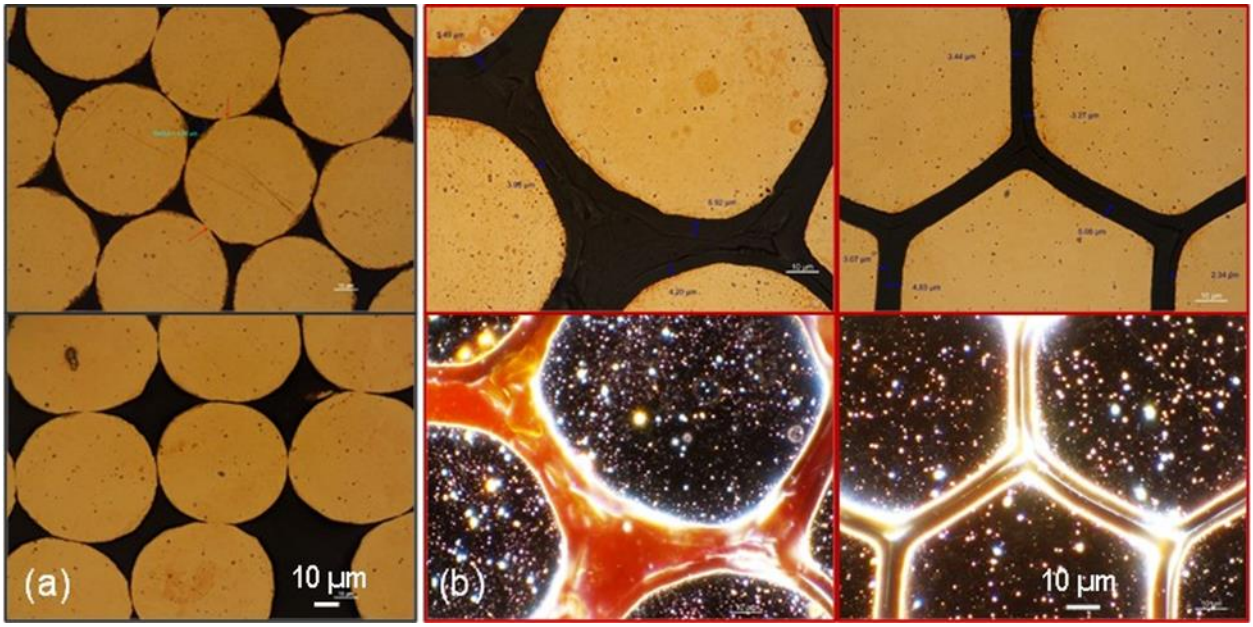

Figure 2. Typical microstructures of Litz wires, (a) typical packing patterns of uncoated Cu filaments in Litz1 and (b) coated filaments of Litz2 wire in either loosely packed or densely packed areas shown in both bright field (BF), top, and dark field (DF) micrographs, bottom.

From extensive image analysis of numerous representative cross-sectional micrographs with ImageJ software, the overall areal fraction of each structural components were determined and summarized in Table 1. With reasonably uniform distribution, the fractions were averaged out of all four bundles randomly in the Litz1wire. In the case of the Litz2 wire, however, they were measured separately per bundle and for either densely packed or loosely packed areas as designated in the right-side picture, and thickness of the coating on CF was also included in the analysis. As expected, the Litz2 wire showed considerable differences between the densely packed areas and the loosely packed areas, particularly the areal fraction of the open spaces. Note that the average thickness of the coating in the densely packed area was clearly reduced from that of the loosely packed area due to the excessive packing force which suggested again that the force was significant. It is also of interest to note that the standard deviations of those fractions were considerably larger in the Litz2 wire, especially in the loosely packed areas, due to its non-uniformity, compared to the Litz1 wire. Finally, the overall areal fraction of all open spaces including the inter-bundle spaces both in center and at four edges which also varied with twisting or winding conditions could be 32% for Litz1 and 21.9% for Litz2 wire in average. These were useful information in developing the alternative VaAIP potting process to be discussed later and also for thermal modeling effort as another major activity performed by the project team, Ref. [1] and [5].

Table 1. Quantitative image analysis results of microstructures of as-received Litz wires.

Litz Wire Type		Areal Fraction			Coating Thickness um
		Cu filament	Coating	Open space	
Litz1	all bundles	75.9% ± 1.2%		24.2% ± 1.2%	
Litz2	B1-1	67.8%	14.2%	18.0%	4.13 ±1.3
	B2-1	60.0%	14.6%	25.3%	4.37 ±1.8
	B3-1	62.0%	15.1%	22.9%	4.23 ±1.0
	B4-1	55.2%	13.8%	31.0%	4.26 ±1.3
	Avg.	61.3% ± 5.2%	14.4% ± 0.6%	24.3% ± 5.4%	4.26 ±0.1
	B1-2	73.2%	16.4%	10.4%	3.77 ±1.0
	B2-2	74.3%	14.9%	10.8%	3.46 ±0.7
	B3-2	75.0%	16.7%	8.3%	3.73 ±0.7
	B4-2	76.1%	16.6%	7.3%	3.66 ±0.8
	Avg.	74.7% ± 1.2%	16.2% ± 0.8%	9.2% ± 1.7%	3.65 ±0.1
	Total Avg.	68.0% ± 8.0%	15.3% ± 1.1%	16.8% ± 8.9%	3.95±0.34

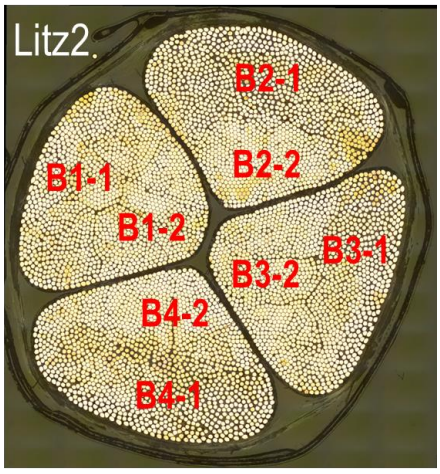

As a part of microstructure analyses, an effort was also made to determine 3-D microstructures of Litz wires for the electro-thermal modeling, particularly to capture wire twisting characteristics. Both μCT scanning and serial polishing, either manually or with automated Robo-Met machine, coupled with high resolution microscopy were explored. The former as an optical sectioning technique was simple and potentially more powerful since no sample preparation was required and it generated thousands of cross-sectional images per mm in a relatively short time. In addition, with properly-written custom analysis software, the thousands of slices can be easily and quickly analyzed using a modestly powerful desktop computer. Figure 3 shows typical images from the μCT scan. While its 3-D images revealed the nature of wire twist clearly, the resolution of the 2-D cross-sections was too poor for any post image analyses whether the entire wire or a single bundle was scanned. For Litz wires with such large metallic volume of CFs, the μCT might not be a good option since extremely high power was required for penetration, thus increasing the focal spot size, and yet still significant scatter was present at the interior regions. On the other hand, the serial polishing coupled with high resolution microscopy provided sequence of high resolution cross-sectional images as a function of z-axis, Figure 4 for the Litz1 wire and Figure 5 for Litz 2 wire, respectively. Those cross-sectional images were zoomable down to micron scale in a computer monitor with good resolution, thus ideal for post image analysis using the ImageJ software. The sequence of cross-sections showed changes in distributions and packing patterns of CFs in terms of axial twisting of wire which can be input directly to the electro-thermal modeling solutions. To capture the effects of twisting on the microstructure, the serial polishing was performed on a wire section longer than ~25 mm. One interesting difference in 3-D microstructure between the two Litz wires was that the shape of the overall cross-section in the Litz2 wire changed from an oval shape to a diamond shape with varying z-axis location while the Litz1 wire maintained the same oval shape throughout the entire section. The overall shape changes, involving changes of both bundles and the inter-bundle open spaces, especially at the center, should be counted for developing the new potting process as well as thermal modeling. It is also of interest to note that a 3-D image comparable to or better than the μCT image, Figure 3(a), can be developed from the slices from the RoboMet, if they were thin enough.

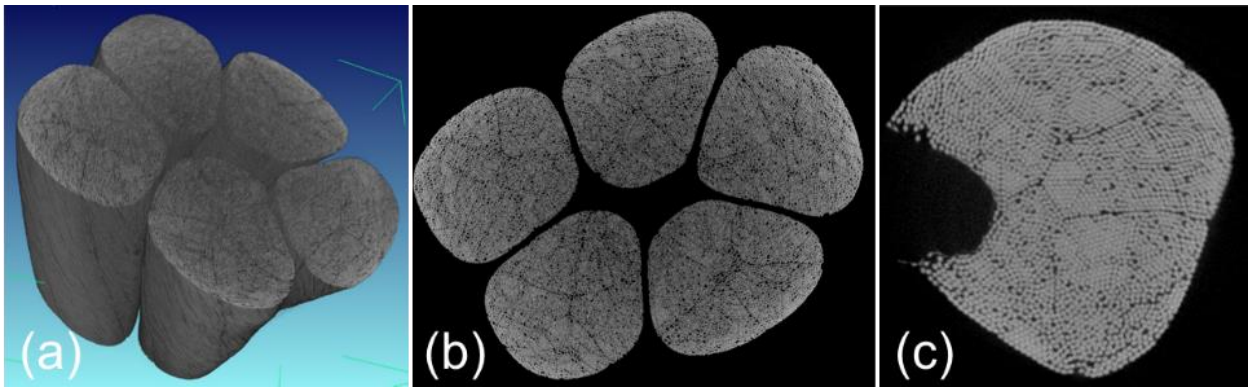

Figure 3. Images from micro-CT scan, (a) 3-D structure of the entire wire section, (b) typical cross-section, (c) typical cross-section when a separated bundle was scanned alone.

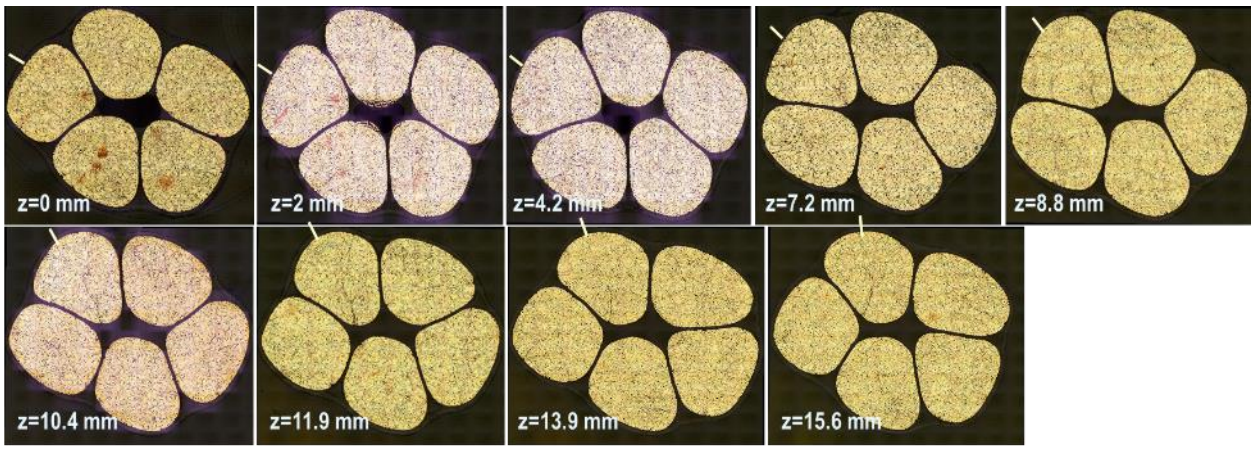

Figure 4. Sequence of cross-sections of Litz1 wire as a function of axial position, z, by manual serial polishing.

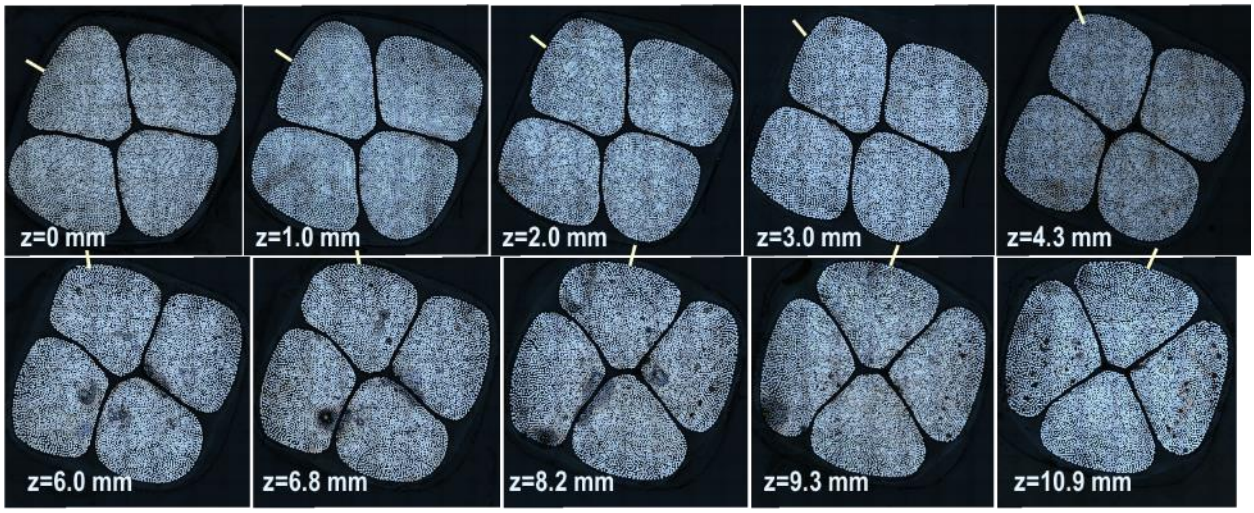

Figure 5. Sequence of cross-sections of Litz2 wire as a function of axial position, z, by automatic Robo-Met serial polishing.

B. Characterization of Packing Pattern

Since the Litz2 wire was selected as the final candidate for the HEMM, Ref. [4], additional quantitative microstructure analysis was performed on its high resolution cross-sectional micrographs to determine more accurate fractions of various CF packing patterns for more effective and accurate thermal modeling. As shown in Figure 6,

two representative cross-sections, oval vs. diamond, were selected for the analysis, and five most common patterns, e.g., hexagonal, parallelogramical, triangular, square/rectangular, and random pattern, were identified based on connectivity and surrounding conditions, key factors affecting heat transfer, even though parallelograms and triangles can be part of hexagons. Utilizing the ImageJ software at a high enough magnification (e.g., 25%), those patterns were deliberately and manually assigned and counted per bundle in the same sequential order listed above, starting from the corner close to the wire center. According to the wire specifications by the manufacturer, the total number of CFs used per bundle was 1500, but it was still counted by the analysis to assess their continuity. The overall results are summarized in Table 2. After the number fractions were determined, their areal fractions were also calculated by measuring area of each bundle. Note that the cross-sectional area of each filament was calculated using the average diameter of conductor filament and coating thickness from Table 1. The changes in fractions of each patterns between the two typical cross-sections was rather small, especially when they were categorized between the ordered, regardless of shape, and the random pattern. Accurately enough though, the fractions of the random pattern and the void or open space in the oval shape were consistently higher than those in the diamond shape which suggested that the latter was supposed to be under higher compaction. The average void content calculated by the pattern analysis was in good agreement with the overall average of 16.8% from the previous image analysis of the as-received cross-sections, Table 1. It was of interest to note that there were slight variations in total number of filament per bundle among different bundles and also between the oval and the diamond shapes even though they were only a few inches apart in the same wire section. That might be due to breakage of filaments during wire construction process. It should be also noted that the realistic number fractions of the various packing patters were essential for more accurate thermal modeling, but at the same time, their distribution modes and boundary conditions can be also considered as equally important inputs for the modeling, if they can be more systematically characterized and quantified.

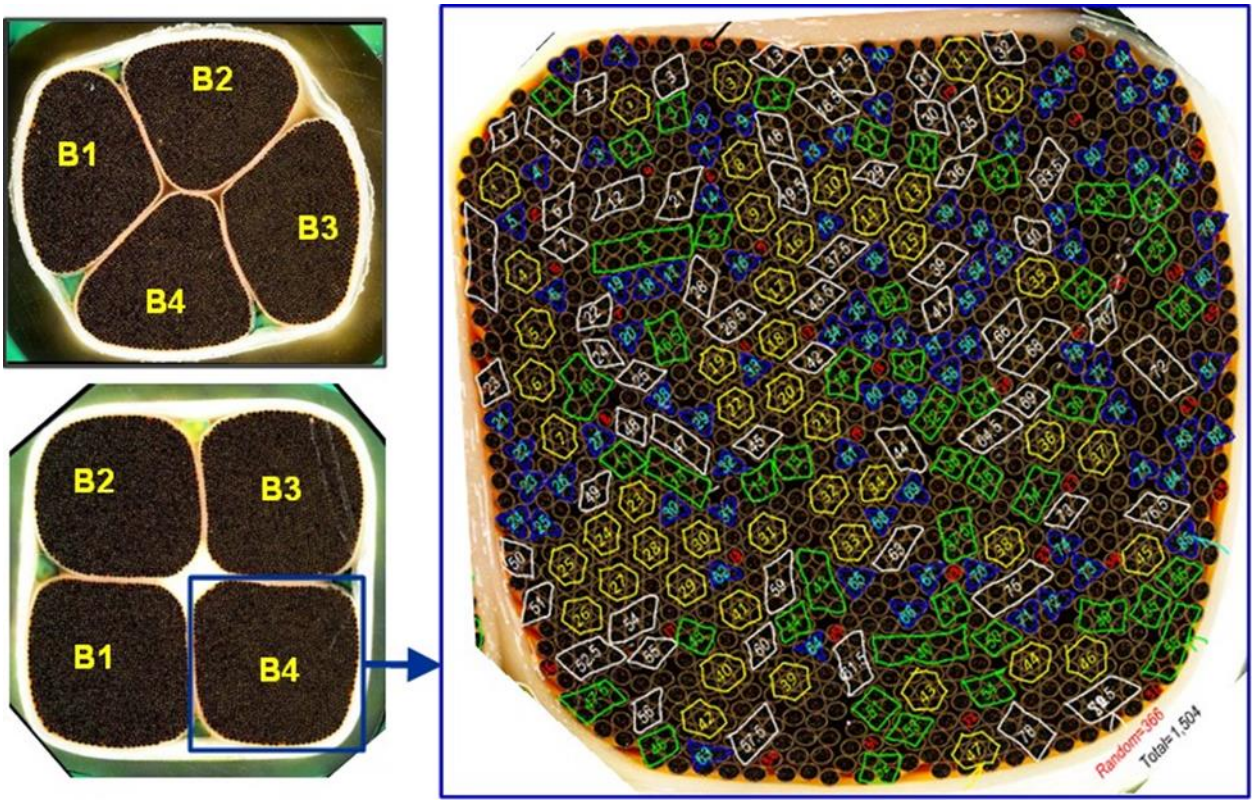

Figure 6. Two typical cross-sectional shapes of Litz2 wire per twisting or winding conditions and quantitative analysis on conductor filament packing patterns.

Table 2. Results of quantitative packing pattern analysis in Litz2 wire. Note that "Void" meant the open spaces between Cu conductor filaments to be filled by potting material.

CS	Bundle #	# of conductor filaments (CF)					Total # of CF	Number Fraction, %					Total Area, mm^2	Areal Fraction (incl. coating), %					
		Hexago	Parallelogram	Rectangle	Triangle	Random		Hexagon	Parallelogram	Rectangle	Triangle	Random		Hexagon	Parallelogram	Rectangle	Triangle	Random	Void
Oval	B1	210	244	288	303	444	1489	14.1%	16.4%	19.3%	20.3%	29.8%	11.4	11.5%	13.3%	15.7%	16.5%	24.2%	18.7%
	B2	525	204	168	192	408	1497	35.1%	13.6%	11.2%	12.8%	27.3%	11.0	29.7%	11.5%	9.5%	10.9%	23.1%	15.3%
	B3	252	232	232	336	447	1499	16.8%	15.5%	15.5%	22.4%	29.8%	11.7	13.3%	12.3%	12.3%	17.8%	23.7%	20.7%
	B4	343	332	212	165	442	1494	23.0%	22.2%	14.2%	11.0%	29.6%	11.0	19.4%	18.8%	12.0%	9.3%	25.0%	15.4%
	AVG	***333***	***253***	***225***	***249***	***435***	***1495***	***22.2%***	***16.9%***	***15.1%***	***16.7%***	***29.1%***	***11.3***	***18.5%***	***14.0%***	***12.4%***	***13.6%***	***24.0%***	***17.5%***
	SD	***140***	***55***	***50***	***83***	***18***	***4***	***9%***	***4%***	***3%***	***6%***	***1%***	***0.37***	***8%***	***3%***	***3%***	***4%***	***1%***	***3%***
Diamond	B1	280	304	248	243	423	1498	18.7%	20.3%	16.6%	16.2%	28.2%	11.5	15.2%	16.5%	13.5%	13.2%	23.0%	18.7%
	B2	308	368	288	219	317	1500	20.5%	24.5%	19.2%	14.6%	21.1%	11.0	17.4%	20.8%	16.3%	12.4%	17.9%	15.2%
	B3	280	278	160	363	419	1500	18.7%	18.5%	10.7%	24.2%	27.9%	11.0	15.8%	15.7%	9.0%	20.4%	23.6%	15.5%
	B4	329	322	232	255	366	1504	21.9%	21.4%	15.4%	17.0%	24.3%	11.2	18.2%	17.8%	12.9%	14.1%	20.3%	16.7%
	AVG	***299***	***318***	***232***	***270***	***381***	***1501***	***19.9%***	***21.2%***	***15.5%***	***18.0%***	***25.4%***	***11.2***	***16.7%***	***17.7%***	***12.9%***	***15.0%***	***21.2%***	***16.5%***
	SD	***24***	***38***	***53***	***64***	***50***	***3***	***2%***	***3%***	***4%***	***4%***	***3%***	***0.21***	***1%***	***2%***	***3%***	***4%***	***3%***	***2%***

C. Vacuum-assisted Axial Injection Potting (VaAIP)

Dipping can be a simplest and effective process technique to pot winding wires in a motor via transverse infiltration of resin through the winding stack, but it may not be the best option for the Litz wires because of their build structure which may restrict transverse resin flow even though the process was reinforced by applying vacuum and pressure such as the vacuum pressure impregnation (VPI) process, Ref. [5]. Therefore, a different approach, namely vacuum-assisted axial injection potting (VaAIP) process, was developed based on the microstructure of the Litz wires discussed earlier. Since the open spaces, either inter-filament or inter-bundle, were continuously channeled through the entire wire length, it was anticipated that the potting resin can easily infiltrate along the channels axially when a high vacuum is pulled through the micro-channels and if viscosity of potting resin is low enough. Furthermore, the process can be enhanced if the wire is preheated, thus the viscosity of the resin is lowered. Figure 7(a) shows the typical experimental setup to prove the concept of VaAIP process on the actual Litz wires. An open aluminum mold (4×7×1.5 inch in dimensions) with "S" shape continuous semi-circular groove (0.5 inch wide × 0.4 inch deep) was designed to mimic the actual motor winding, especially by introducing both horizontal and vertical curvatures with 1.0 inch outer radius. The total wire length used in the initial trials with the mold was about 30 inch (0.76 m) long. In order to pull a high vacuum inside, the Litz wire was sealed from atmosphere with either Nylon vacuum bagging film (for the first trial with Litz1) or Polyolefin clear shrink tubing (for the second trial with Litz2) in its entirety except both ends before mounting into the mold. The shink tubing made the setup preparation much easier and more practical since it just needed quick recovery/shrink at 121 °C for 30 minutes and provided a good sealing. Then, the sealed wire was installed into the mold while keeping the maximum twist on the wire section. At the same time, the wire was connected to a resin dispenser on one end and to vacuum pump on the other end using a Tygon vacuum tubing. Both connections were finished with air-tight sealing using vacuum sealing tape, but great care was taken to keep the ends of the Litz wire open as clear as possible for smooth and full resin flow. The setup was placed on a hot plate and its temperature was monitored with a thermometer.

The Durapot™ 863 epoxy was mixed by centrifugal de-aeration process using the Thinky mixer (Think U.S.A., Inc., CA) with an optimized condition followed by degassing in a vacuum oven to minimize any trapped air. The mold and the resin were pre-heated to 60 - 70 °C prior to injection to lower its viscosity, thus to enhance the process. A high vacuum up to 29.5 inHg was maintained on inside of the Litz wire before and during resin injection. Figure 7(b) shows the front line of resin infiltration during the process where clear color change was visible, thus the status of the infiltration process was monitored. More resin batches were prepared at the same manner and added into the dispenser unitl the infiltration process was completed. Once the process was completed, both ends were clamped on vacuum tubing and disconnected from the resin dispenser or vacuum line. The potted epoxy in the wire assembly was cured within the mold at 250°F/121°C for 4 hours in either an autoclave with 45 psi hydrostatic pressure for the Litz1 trial or a conventional air-circulated oven for the Litz2 trial.

During the VaAIP process, the amount of injected resin was regularly monitored as a function of time via reading the scale on the resin dispenser and plotted in Figure 8 for the initial trials with Litz1 or Litz2 wire. Note that the process conditions between the two trials differed slightly as listed in the plots. The plots also displayed the estimated

amounts of resin needed to fill the voids or open spaces calculated based on their overall areal/volume fractions, 32% for Litz1 and 21.9% for Litz2 wire, including the inter-bundle spaces both in center and at four edges from the microstructure analysis described earlier. With the void volume fractions, the overall dimensions of the 30 inch long wire section, and the estimated density, ~1.0 g/cc, of the mixed resin, they were 14.4 g for Litz1 and 8.2 g for Litz2 wire, respectively. From the left hand graph, amount of resin vs injection time, the injection rate of both cases seemed to be similar, but when they were plotted in terms of specific amount of resin per void volume in the right, it was clear that the injection rate in the Litz2 trial was significantly faster, thus the maximum infiltration was achieved much quicker even though the total amount of injected resin at the end of the process was about same in both cases. On the other hand, the overall weight of the 30 inch long wire sections used in ther trials was also measured before and after the VaAIP process, and found that the total amount of the injected resin was 12.2 g for Litz1 and 11.2 g for Litz2 wire. While those were reasonably well-matched with the injection rate plots at the end of the process, Figure 8, in both cases, the latter case of Litz2 trial showed a better chance for more complete infiltration with higher fill% since the total injected resin amount, 14 g, was significantly more than the amount needed to fill the voids, 8.24 g.

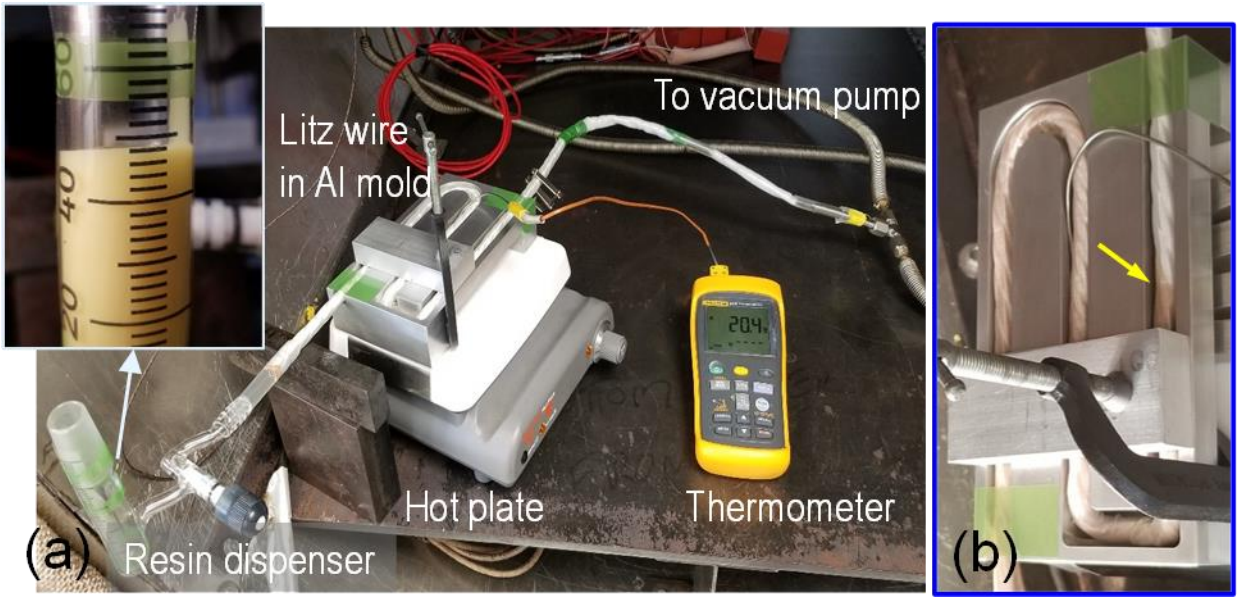

Figure 7. (a) Typical experimental setup for VaAIP process and (b) resin infiltration front shown as color change at the arrow mark.

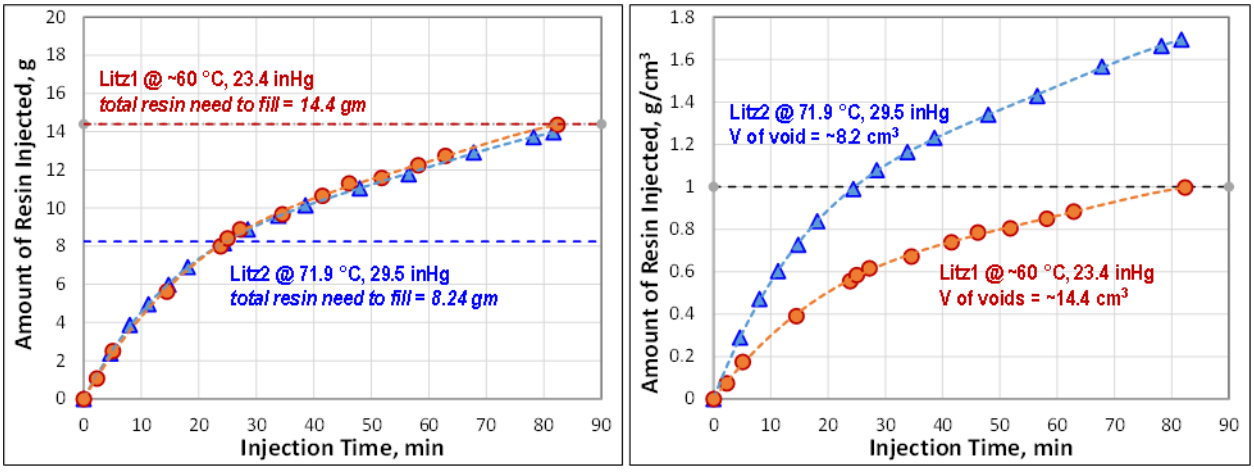

Figure 8. Injection rate comparison between two VaAIP processes with Litz1 or Litz2 wire. Note that the right hand graph was plotted in terms of specific amount of resin injected per void volume, g/cm³.

In order for more accurate and direct potting quality assessment, physical sectioning of the VaAIP processed wires was conducted at various locations. Typically, seven cross-sections were obtained from various locations of the 30

inch-long Litz wire starting from the injection port, i.e., at 1 inch, at 7 inch, at 11-12 inch within the horizontal curvature, at 14-16 inch, at 18-20 inch within the vertical curvature, at 20-22 inch, and at 28-29 inch. The sections were then encapsulated with a fluorescent epoxy and metallurgically polished to obtain clear cross-sectional microstructures. The anatomy of cross-sections are presented in Figure 9 and Figure 10 for Litz1 and Litz2 trial, respectively. As indicated by 3-D microstructure analsyis, the cross-sectional shapes including those of individual bundles as well as inter-bundle center or edges changed with location due to changes in twisting or mounting conditions, significantly more in Litz2 wire.

Figure 9. Anatomy of VaAIP processed Litz1 wire.

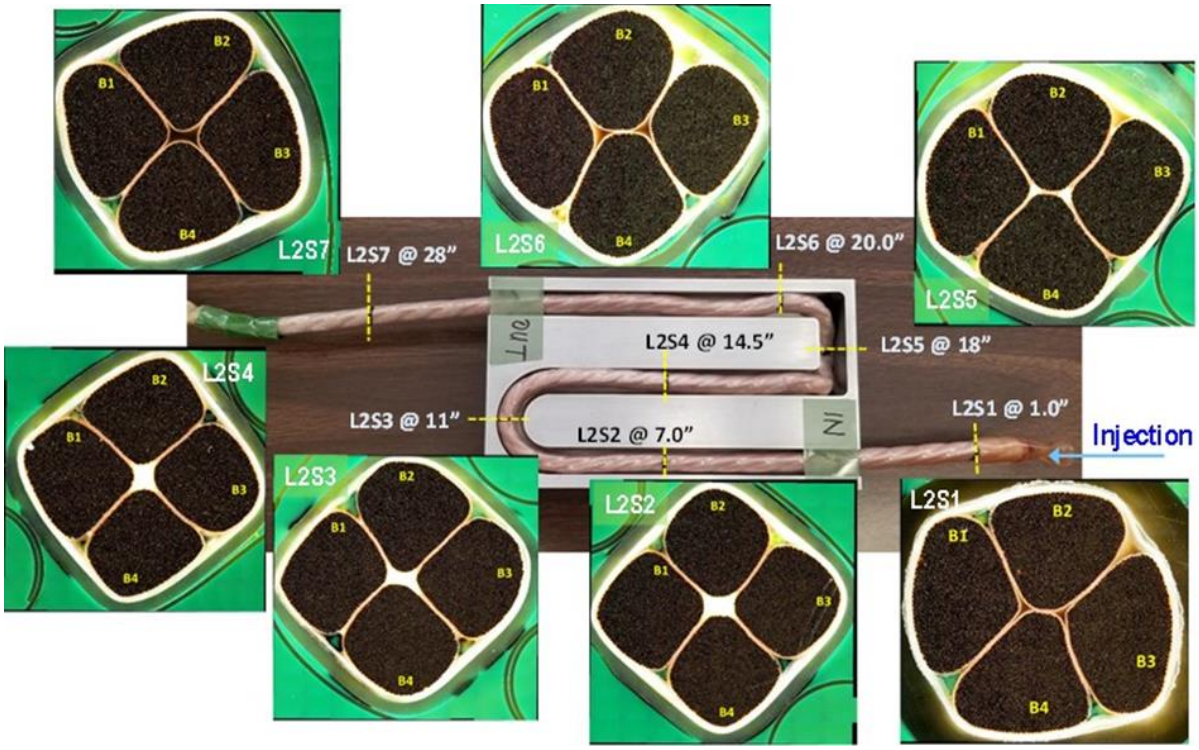

Figure 10. Anatomy of VaAIP processed Litz2 wire.

On each cross-section, extensive statistical microstructure analysis at high magnification, typically 1500x, using NIKON ECLIPSE MA200 high power microscope was performed to quantify potting quality in terms of fill % by directly measuring void areas. The voided area, which was either empty or filled with the fluorescent epoxy, and the potted area were clearly distinguishable since they showed different light reflection under different mode, either bright field or dark field, of the optical microscope. The conditions and procedure of the microscopic and statistical analysis were optimized and standardized for all cross-sections and wire types, thus more representative and comparable values were obtained. The fill % calculations were conducted separately for (i) inter-bundle center, (ii) inter-bundle edge area, and (iii) Intra-bundle area. For (i) and (ii), all the areas were measured directly, but for (iii), the measurement was done selectively, thus statistical, by scanning about 30% of area per bundle randomly but systematically. The overall results are summarized in Figure 11 and Figure 12 for Litz1 and Litz2 trial, respectively.

In the case of the Litz1 trial, the fill % for the inter-filament open spaces within each bundle ranged between 55 and 90 %, the lowest being at specific locations, e.g., at 7 inch and 20 inch from the injection point, and the trend was similar in most bundles. The good-sized inter-bundle center area was mostly filled by 100 % except two locations at 7 inch and 29 inch from the injection point again. However, all of the inter-bundle edge areas were not well-filled regardless of axial location, but it was suspected that the edges of wire were somewhat blocked by sealing tape apllied between the bagging film and vacuum tubing. Other key findings included; (i) the filling state was independent on size of inter-filament spacing, (ii) horizontal curvature did not cause any blockage on resin flow, but the vertical curvature seemed to cause some flow blockages and more trapped air pockets for the lower fill %, (iii) flow through inter-bundle center was not affected by either curvature, (iv) data indicated poor transverse resin flow across bundles or filaments. In general, large fluctuations in fill % in the Litz1 wire might be due to some trapped air bubbles causing non-uniform vacuum state, but regardless of any flow blockages, the resin seemed to find ways to flow around to reach the end of the wire section resulting in a reasonably high fill %.

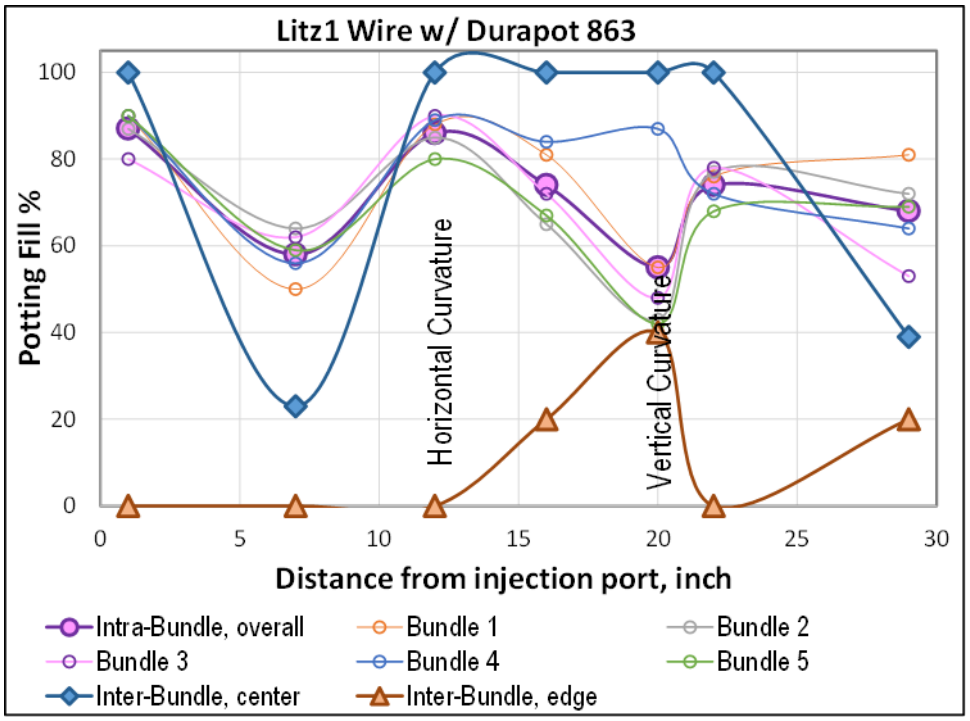

Figure 11. Potting fill percent of Litz1 wire at various locations after VaAIP process.

As expected from the resin injection rate analysis earlier, the second VaAIP trial with Litz2 wire achieved much higher potting fill % in all areas, i.e., 100% in inter-bundle center at all axial locations, 30 – 100% in inter-bundle edges with a trend of increasing with increasing distance from the injection point, and greater than 99.6% in intra-bundle area for most bundles regardless of packing density, axial location or twist angle. The overall improved potting quality of Litz2 wire ought to be attributed by its microstructure, e.g., larger filament diameter, thus larger inter-filament open spaces and lower packing density, especially outer bundle area, as well as the improved VaAIP process, e.g., higher vacuum, better control of preheat temperature to lower viscosity, or better sealing with heat shrink tubing etc.. The PI coating present on Litz2 wire might affect resin flow pattern, thus contributed to the improved potting

quality, but the effects shall be experimentally validated. It was also apparent that the process was not affected by either horizontal or vertical curvature in terms of any blockage on resin flow or excessive trapped air pockets. However, the poor fill% of all inter-bundle edges suggested poor transverse resin flow across bundles in radial direction which was consistent with the finding from the Litz1 trial. From the comprehensive analyses, it was concluded that the VaAIP process was promising and it could be potentially better than other conventional methods for achieveing high quality potting in the Litz wires. Overall, the concept was validated.

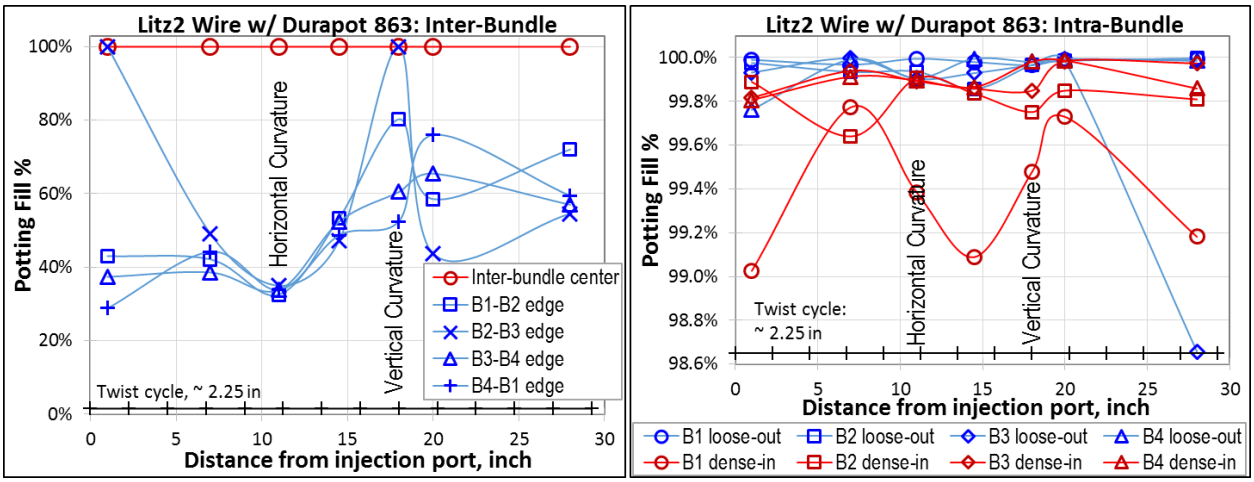

Figure 12. Potting fill percent of Litz2 wire at various locations after VaAIP process. Note that the twist cycle of the Litz2 wire was about 2.25 inch.

In addition, it was noticed from the cross-sectional micrographs, Figure 10, that color of the potted epoxy, particularly in the inter-bundle center area, varied from dark brown to light yellow or white depending on axial location. The cross-sections near the ends, e.g., L2S1, L2S6, and L2S7, was the former while most cross-sections in mid axial locations showed the latter. Based on high magnification microscopic examination, morphology of their polished surfaces was also different, e.g., smooth clean texture from the dark brown colored L2S7 cross-section vs. dusty rough texture from the light yellow colored L2S2 cross-section as shown in Figure 13. With a suspicion of abnormal cure of the resin as a cause, a systematic FT-IR analysis was performed on those epoxy surfaces.

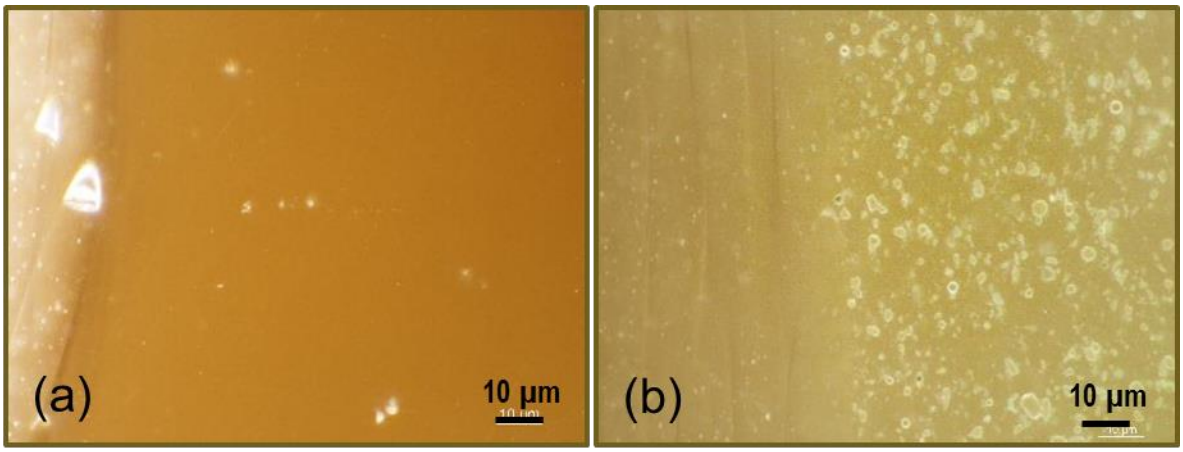

Figure 13. High magnification micrographs of inter-bundle center area from (a) L2S7 and (b) L2S2.

As summarized in Figure 14(a), the light yellow colored surfaces involved with two or three distinct IR peaks at around 1800 wavenumbers while the dark brown colored surface was identified by one IR peak in the same wavenumber region. Such changes in IR spectra was easily explained by the changes in cure state of the potting epoxy represented in terms of cure conditions, i.e., as a function of cure time at 120 °C, Figure 14(b). With increasing the degree of cure, its IR spectra changed from multiple peaks to one peak upon completion of cure. Thus, it was concluded that the light yellow to light brown color was caused by incomplete cure of the epoxy. Since the epoxy was not fully cured, it could be somewhat soft or ductile, thus the conventional metallurgical polishing could not

achieve a smooth clean surface but irregular rough surface as shown in Figure 13(b). This lead to another question whether or how cure reaction of the Durapot™ 863 potting epoxy was deterred in the Litz2 wire, provided that the cure cycle of the part was controlled properly. Since there are no major material differences between the two Litz wire types, except PI wire coating, the exact reasons of curing deterance were not known at the moment, but the cure conditions have to be re-optimized for the Litz2 wire becasue the potted epoxy won't provide full mechanical integrity or thermal stability if it were not fully cured.

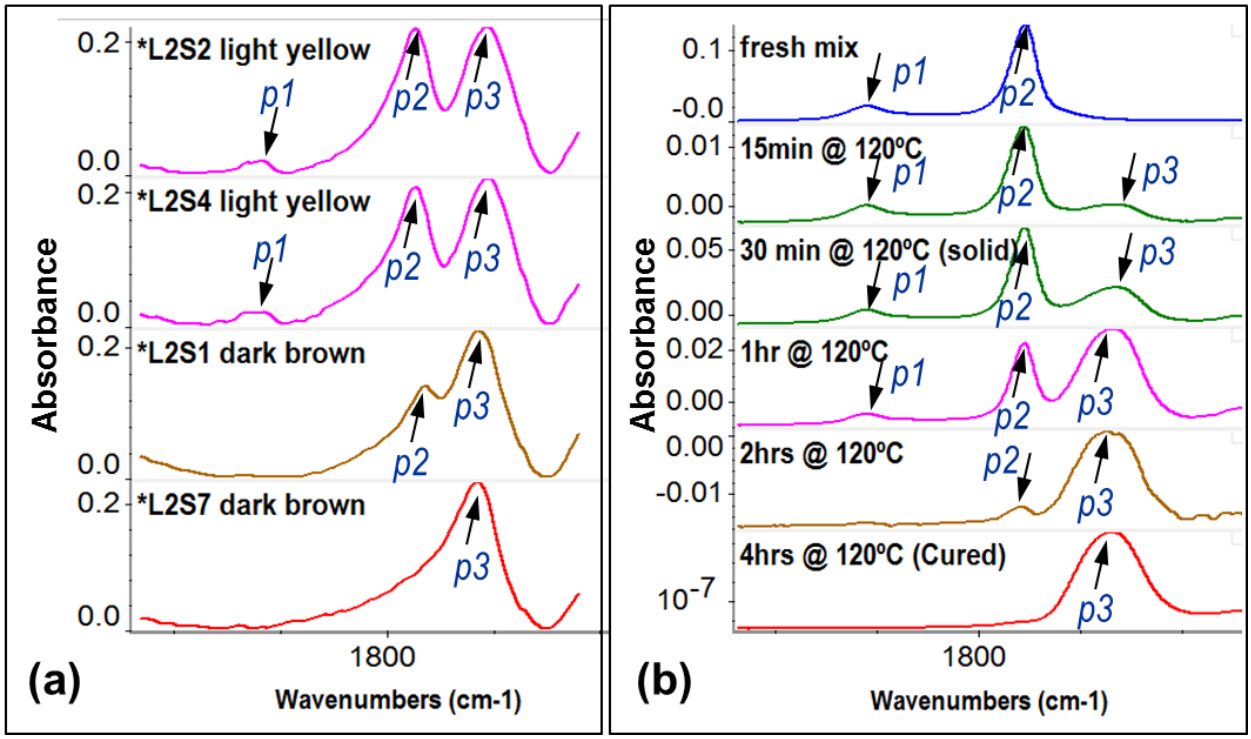

Figure 14. FT-IR spectra of the potting epoxy after (a) VaAIP process with Litz2 wire at various locations and (b) various cure stages as a function of cure timeat 120 °C, thus the degree of cure.

IV. Summary and Conclusions

As the initial effort of pot-ability assessment, configuration and microstructure of the candidate Litz wires, particularly packing patterns and distribution characteristics of CFs and inter-filament open spaces, such as dimensions and overall areal or volume fraction, were determined successfully.

- Distribution of CFs was generally homogenous in Litz1 but Litz2 wire formed two distinctive patterns, i.e., denser packing in inner area vs. loose packing in outer area of bundles regardless of sample preparation or mounting conditions. Some CFs in the former area were deformed into hexagonal shape only separated by wire coating under substantially high packing forces.
- The average areal fraction of all open space per wire cross-section was 32% for Litz1 and 21.9% for Litz2 wire while the fraction per bundle was 24.2±1.2% for Litz1 and 24.3±5.4% or 9.2±1.7% for densely packed or loosely packed area of Litz2 wire, respectively.
- 3-D microstructure of Litz wires obtained by serial polishing and high resolution microscopy showed changes in shape and microstructures of bundles and overall cross-sections with axial twisting that can be untilized in the electro-thermal modeling.
- Packing patterns of CFs in either random or various ordered patterns were fully characterized and quantified for the Litz2 wire, and the results were used in the electro-thermal modeling.

An alternative process technique, namely vacuum-assisted axial injection potting (VaAIP), was developed to pot the Litz wires in the stator winding of high power density electric motors for the future electrified aircrafts.

- Two elaborate experimental trials with the Durapot™ 863 potting epoxy on 30 inch long Litz wires involving representative winding curvatures were performed successfully to validate the VaAIP concept.

- With improved VaAIP process techniques and more favorable microstructure, significantly better potting quality was achieved from the Litz2 wire.
- Based on the results of the trials, it was concluded that the VaAIP process was promising and it could be potentially better than other conventional methods for achieveing high quality potting in the Litz wires.

V. Future Work Plan

Even though the concept of VaAIP process has been proved experimentally, in order to implement this new process to the actual motor windings, it will require further modifications and optimizations of the process inclduing a full-scale component or subsystem demonstration. To maximize its thermal performance, thus the motor performance, an effort is also planned to enhance thermal conductivity of the Durapot™ 863 epoxy resin by adding conductive nano fillers, while maintaining its good processability. The following specific tasks are planned for future development and improvement:

- Evaluation of cure behavior of the potting epoxy in conjunction with Litz2 wire and re-optimization of cure conditions
- Modification of the potting resin with BNNS nanofillers by investigating their effects on not only thermal conductivity and dielectric strength but also viscosity, cure behavior, and degree of dispersion as a function of loading rate. Initial efforts will be made (i) to develop and optimize the mixing method and procedure and (ii) to characterize and quantify the degree of nanofiller dispersion
- Scale up the VaAIP process using a full-size component scale statorette representing a high power motor, e.g., HEMM
- Evaluation of mechanical stability and durability of the potting resin cured in Litz wires

Acknowledgments

The author would like to thank Dan Scheiman, Paula Heimann, Rich Martin, Joy Buehler, Pete Bonacuse, Rick Rauser, and Tim Ubienski for their technical contributions, and acknowledge Andrew Woodworth as a project lead and for reviewing this paper, and the rest of project team for their supports. This work has been sponsored by NASA's Advanced Air Transport Technologies (AATT) Program under the Aeronautics Research Mission Directorate (ARMD).

References

[1] Woodworth, A., Jansen, R., Duffy, K. P., Naghipour, P., & Shin, E. E., "Creating a multifunctional composite stator slot material system to enable high power density electric machines for electrified aircraft applications," Proceedings of the AIAA/IEEE Electric Aircraft Technologies Symposium (EATS), 12 - 13 July, 2018, Cincinnati, OH. https://doi.org/10.2514/6.2018-5012

[2] New England Wire Technologies website, https://www.newenglandwire.com/litz-wire-benefits-and-applications/.

[3] Roth, D., Rauser, R., Shin, E. E., Burke, C., "Fine Scale Metrology on Cylindrical Structures Using X-ray Micro-computed Tomography" Materials Evaluation, VOL. 73, No. 5, May 2015, pp. 611-620.

[4] Jansen, R., DeJesus Arce, Y., Kascak, P., Dyson, R., Woodworth, A., Scheidler, J., Edwards, R., Duffy, K., McCormick, S., Passe, P., "High Efficiency Megawatt Motor Conceptual Design", Proceedings of the AIAA/IEEE Electric Aircraft Technologies Symposium (EATS), 2018 Joint Propulsion Conference, 9 - 13 July, 2018, Cincinnati, OH. Published Online:8 Jul 2018, https://doi.org/10.2514/6.2018-4699

[5] Woodworth, A., Sixil, W., Edwards, R., Jansen, R., McCormick S., Robbie, M., Smith, A., Naghipour, P., & Shin, E. E., "Thermal Characterization of Potted Litz Wire for High Power Density Aerospace Applications," Proceedings of the AIAA/IEEE Electric Aircraft Technologies Symposium (EATS), 22 - 24 August, 2019, Indianapolis, IN.